Engineering Geology 304 (2022) 106677

Contents lists available at ScienceDirect

Engineering Geology

journal homepage: www.elsevier.com/locate/enggeo

Random finite element analysis on uplift bearing capacity and failure mechanisms of square plate anchors in spatially variable clay

Xue-Jian Chen [a,c], Yong Fu [b,d,*], Yong Liu [a]

[a] State Key Laboratory of Water Resources and Hydropower Engineering Science, Institute of Engineering Risk and Disaster Prevention, Wuhan University, Wuhan 430072, PR China
[b] Department of Ocean Science and Engineering, Southern University of Science and Technology, Shenzhen 518055, China
[c] Department of Civil and Environmental Engineering, National University of Singapore, 117576, Singapore
[d] Southern Marine Science and Engineering, Guangdong Laboratory (Guangzhou), Guangzhou 511458, China

ARTICLE INFO

Keywords:
Square plate anchor
Random finite element analysis
Spatial variability
Uplift bearing capacity
Failure mechanism

ABSTRACT

Square plate anchors are increasingly used to provide uplift bearing capacity for both onshore and offshore infrastructures. Past research on the behavior of plate anchors mostly assumed that the soil strength is uniform or linearly increasing with depth without considering the geological uncertainty due to soil spatial variability. This study therefore conducted a series of three-dimensional random finite element analyses on the uplift bearing capacity and failure mechanisms of square plate anchors considering the combined effects of anchor buried depth and soil spatial variability. It was found that two typical types of failure mechanisms, namely, a localized rotational scoop failure mechanism and a global shear failure mechanism would form in random soils with relatively weak and strong soil strengths, respectively. A larger buried depth of at least $3B$ (B = width of plate anchor) is required to ensure a localized failure mode in random soils. Moreover, the mean uplift bearing capacity in random soils is generally lower than the corresponding deterministic value. For this reason, the deterministic uplift bearing capacity is generally overestimated. Finally, this study provided a quantitative approach to predict the probability of failure for plate anchors considering the combined effects of anchor buried depth and soil spatial variability, which may benefit the estimation of the probability of failure for square plate anchors as part of the conventional factor of safety design approach.

1. Introduction

Plate anchors, such as suction embedded plate anchors (SEPLA) (Randolph et al., 2011) and vertically loaded anchors (VLA) (Xing et al., 2021) in Fig. 1, are widely used to provide uplift bearing capacity for offshore oil platforms (see Fig. 2), due to their advantages in cost saving, rapid installation and accurate positioning (Wang et al., 2010). Plate anchors are usually installed at the designed depth (H) within the seabed to bear the uplift loads (Liu et al., 2018a), as shown in Fig. 2(a). Currently, various shaped plate anchors have been reported, e.g., strip, square, circular and rectangular plate anchors. As reported by Wilde et al. (2001), the dimensions of plate anchors are usually 2.5–3.0 m in height, 6.0–7.3 m in width for temporary installations and 4.5 m in height, 10.0 m in width for permanent installations.

The performance of a plate anchor is commonly estimated by its ultimate uplift resistance (Q_u), which can be expressed in the form of the uplift bearing capacity factor (N_c) (Das, 1978; DNV, 2017):

$$N_c = \frac{Q_u}{A s_{u0}} \tag{1}$$

where A is the bottom area of a plate anchor; s_{u0} is the undrained shear strength of soil at the depth of the plate centroid. As shown in Fig. 2(b) and (c), the undrained shear strength (s_{u0}) of clay is assumed to be uniform or linearly increasing with soil depth (z) (Song et al., 2008; Liu et al., 2018a):

$$s_{u0} = \begin{cases} s_{um}, \text{for homegeneous clay} \\ s_{um} + kz, \text{for non-homegeneous clay} \end{cases} \tag{2}$$

where s_{um} is the undrained shear strength at the mudline level; k is the gradient of undrained shear strength with soil depth.

The uplift bearing capacity factor (N_c) in Eq. (1) is typically associated with the shape of the plate anchor, buried depth (H), anchor

* Corresponding author at: Department of Ocean Science and Engineering, Southern University of Science and Technology, Shenzhen 518055, China.
E-mail addresses: chenxj@whu.edu.cn (X.-J. Chen), fuy3@sustech.edu.cn (Y. Fu), liuy203@whu.edu.cn (Y. Liu).

https://doi.org/10.1016/j.enggeo.2022.106677
Received 28 October 2021; Received in revised form 11 March 2022; Accepted 16 April 2022
Available online 22 April 2022

inclination angle (β) and soil strength profile (s_{u0}) (Wang et al., 2010; Liu et al., 2018a). Table 1 summarizes research undertaken over the past few decades on the uplift bearing capacity of plate anchors with various shapes, buried depths and soil strengths using different research methods, e.g., experiment, limit analysis and finite element approach. For example, Das (1978, 1980); Das et al. (1985); Das and Puri (1989) conducted a series of physical model tests of plate anchors considering the effects of anchor shape, inclination and soil property and proposed a procedure to estimate the undrained uplift bearing capacity. Merifield et al. (2001, 2003, 2005) and Yu et al. (2015) performed two- or three-dimensional (2D or 3D) limit analyses on the uplift bearing capacity of the plate anchors with varying shapes in both homogeneous and non-homogeneous clayey soils. In addition, investigations on the plate anchors using both small-strain finite element analysis (SSFE, Rowe and Davis, 1982; O'Neill et al., 2003; Yang et al., 2010; Yu et al., 2011; Liu et al., 2018a; Feng et al., 2020) and large-deformation finite element analysis (LDFE, Song et al., 2008; Wang et al., 2010; Chen et al., 2013; Liu et al., 2014a; Tho et al., 2013) are widely reported. Recently, the discrete element method (DEM, Evans and Zhang, 2019; Zhang et al., 2020) has been applied to elucidate the microscale physical processes that influence the overall system behavior of plate anchors. It is noted that the research outlined above assumed a soil condition with constant or linearly increasing soil strengths with depth (i.e., Fig. 2b and c) without consideration of the influence arising from the spatial variability of the soil.

However, natural soil often exhibits inherent spatial variability with non-uniformly distributed material properties due to the complex deposition process of soil (Phoon and Kulhawy, 1999; Cassidy et al., 2013). According to past research (e.g., Srivastava and Babu, 2009; Jiang et al., 2014; Huang et al., 2017), the spatial variability of soil has been widely regarded as one of the primary sources of geological uncertainty, which will significantly affect the behavior of geotechnical structures, such as plate anchors. As reported by Li et al. (2015), the spatial variability of soil strength has an evident effect on the failure

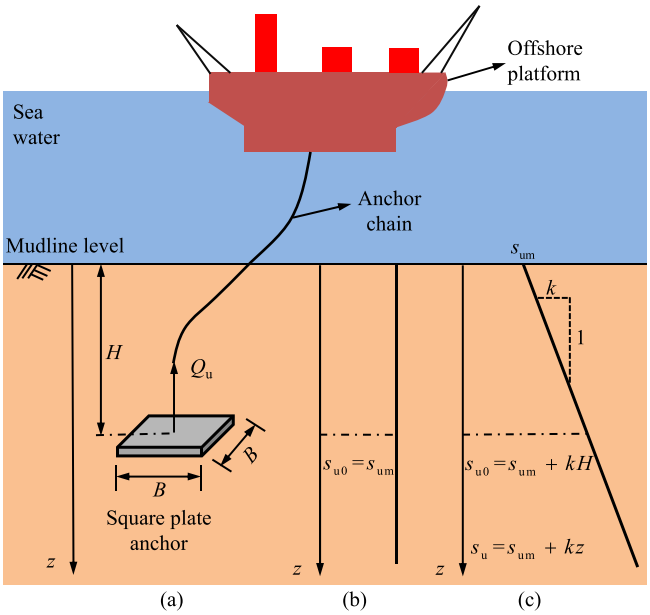

Fig. 2. Problem definition: (a) uplift process of a square plate anchor; (b) seabed profile with uniform undrained shear strength (homogeneous clay); (c) seabed profile with linearly increasing undrained shear strength with soil depth (non-homogeneous clay).

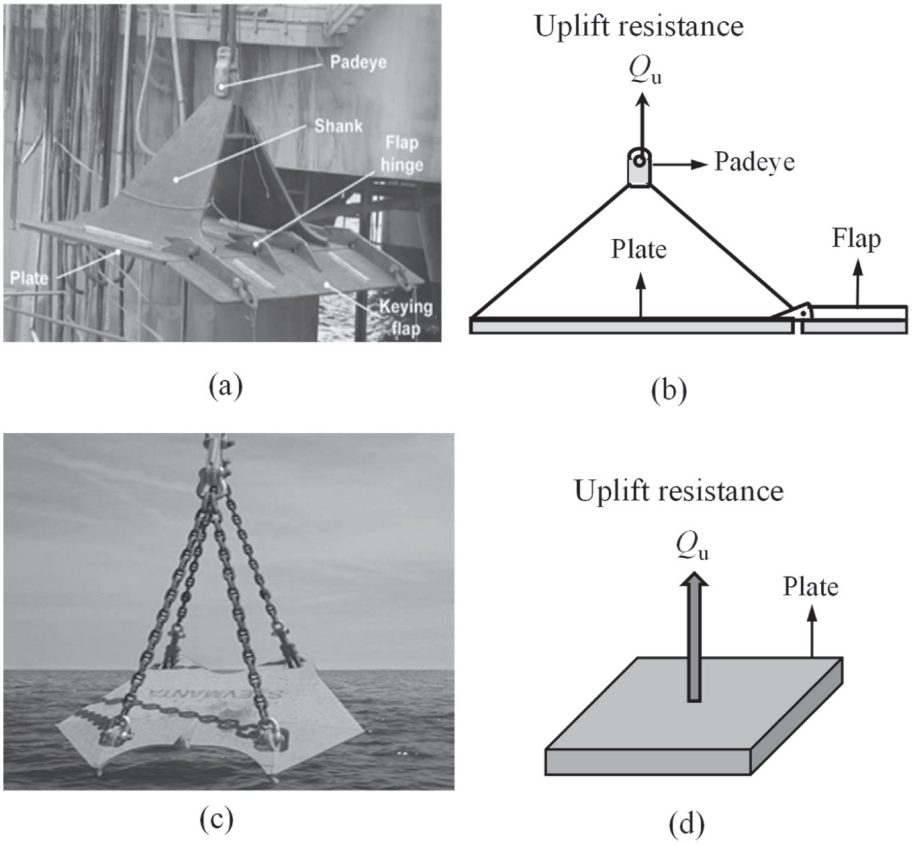

Fig. 1. Schematic diagrams of plate anchors: (a) SEPLA modified from Randolph et al. (2011); (b) simplified SEPLA for analysis; (c) VLA modified from Xing et al. (2021); (d) simplified VLA for analysis.

Table 1
A summary of typical investigations on the uplift bearing capacity of plate anchors.

Plate type	Research methods	Soil type	Soil spatial variation	References
Circular, square, rectangular	Model tests	Homogeneous $k = 0$	No	Das (1978, 1980); Das et al. (1985)
Square	Model tests	Homogeneous $k = 0$	No	Das and Puri (1989)
Strip	LB, UB	Non-homogeneous $k \neq 0$	No	Merifield et al. (2001)
Square, circular, rectangular	LB	Homogeneous $k = 0$	No	Merifield et al. (2003)
Strip	LB, UB	Homogeneous $k = 0$	No	Merifield et al. (2005)
Strip	LB, UB	Non-homogeneous $k \neq 0$	No	Yu et al. (2015)
Strip	Model tests, SSFE	Homogeneous $k = 0$	No	Rowe and Davis (1982)
Strip	SSFE	Non-homogeneous $k \neq 0$	No	Yu et al. (2011)
Rectangular	SSFE	Homogeneous $k = 0$	No	O'Neill et al. (2003)
Square, rectangular	SSFE	Non-homogeneous $k \neq 0$	No	Liu et al. (2018a)
Rectangular	SSFE	Homogeneous $k = 0$	No	Yang et al. (2010)
Square	SSFE	Layered soil	No	Feng et al. (2020)
Strip, circular	SSFE, LDFE	Non-homogeneous $k \neq 0$	No	Song et al. (2008)
Square, strip, circular, and rectangular	SSFE, LDFE	Homogeneous $k = 0$	No	Wang et al. (2010)
Square	LDFE	Homogeneous $k = 0$	No	Chen et al. (2013)
Square	LDFE	Non-homogeneous $k \neq 0$	No	Tho et al. (2013)
Circular, rectangular	LDFE	Non-homogeneous $k \neq 0$	No	Liu et al. (2014a)
Square	DEM	Sand	No	Evans and Zhang (2019); Zhang et al. (2020)
Rectangular	SSFE	Non-homogeneous $k \neq 0$	Yes	Cai et al. (2022)

Note: LB, limit bound analysis; UB, upper bound analysis; SSFE, small-strain finite element analysis; LDFE, large-deformation finite element analysis; DEM, discrete element method. $k = 0$ represents a constant undrained shear strength profile with soil depth while $k \neq 0$ stands for a linearly increasing undrained shear strength profile with soil depth.

mode and bearing capacity of strip footings because the shear band is prone to develop in weaker soils. A 20–30% decrease in the bearing capacity of a strip foundation was also observed in spatially random soils by Griffiths et al. (2002), compared with that in uniform soils. Moreover, Liu et al. (2018b) found that the neglect of the spatial variability of soil strength will result in an unconservative solution for structure design. For example, the deterministic analysis with uniform soil strength yielded an overestimated bearing capacity and the probability of failure for a foundation in spatially variable soil was severely underestimated (Griffiths et al., 2002; Li et al., 2016). Therefore, this highlights the importance and necessity to consider the spatial randomness of soil strength in the design of the uplift bearing capacity of a plate anchor.

To examine the effect of spatial variability of undrained shear strength on the statistics of uplift bearing capacity, Cai et al. (2022) conducted 3D random SSFE analyses on a plate anchor buried in spatially variable clay. The results showed that the undrained uplift bearing capacity of a 3D plate anchor is highly dependent on the level of coefficient of variability (COV) and scale of fluctuation of soil strength. However, the anchor was assumed to be deeply buried with a constant embedment depth of $6B$ (B = width of plate anchor). The effect of buried depth on the uplift bearing capacity and failure mechanism of plate anchors in spatially variable soil remains unknow. To the authors' best knowledge, no other similar studies have been undertaken to quantify the combined effects of buried depth and spatial variability of soil strength on the uplift bearing capacity, failure mechanism, and the probability of failure of a plate anchor.

Therefore, with the purpose of investigating the combined effects of soil spatial variability and anchor buried depth, this study carried out a series of 3D nonlinear random SSFE analyses on the uplift bearing capacity and failure mechanisms of a horizontal square plate anchor with different buried depths in spatially variable clay. The established SSFE model was first validated with the existing numerical solutions in uniform soils. Then, this validated model was used to investigate the effects of soil non-homogeneity (i.e., kB/s_{u0}) and spatial variability (i.e., s_u) on the failure mechanism and uplift bearing capacity of a square plate anchor. Based on the results from the SSFE analyses, a quantitative approach was used to predict the probability of failure for plate anchors considering the combined effects of anchor buried depth and soil spatial variability, which is currently lacking in the public domain. This study can enrich the current database about the behavior of plate anchors in spatially random soil and improve the current design methods for plate anchors.

2. Three-dimensional nonlinear SSFE model

2.1. SSFE model detail

Fig. 3 illustrates the established 3D SSFE model containing a square plate anchor and a soil domain in ABAQUS/Standard (Dassault Systémes, 2018). The parameters used in the SSFE model and the soil properties are listed in Table 2. From the prospective of design, the dimensions of plate anchors are highly dependent on the design loads, soil properties, number of anchors, and design standard. In this study, the width (B) of the square plate anchor is taken as 4 m. This geometry represents a typical size of a buried plate anchor in the field (Wilde et al., 2001), but the exact value selected here is not expected to affect the normalized results presented later in this study. The soil domain is chosen as $5B$ in length, $5B$ in width and $10B$ in height, which is proved sufficient to avoid the boundary effects based on numerical trials on the size of the soil domain. Following Wang et al. (2010), the anchor thickness (t) is set as $B/20$. In the modelling, the square plate anchor is oriented horizontally and wished-in-place at five different buried depths, i.e., $0.5B$, $1.0B$, $2.0B$, $3.0B$, and $4.0B$, respectively. For the scenario with a buried depth greater than $4B$, the embedment effect on the uplift bearing capacity of the square plate anchor is negligible (Wang et al., 2010) and hence is not further examined. Note that a plate anchor in the field is usually installed with the aid of suction caisson. Owing to the keying process, the plate anchor is commonly buried in the seabed with a certain inclination to the horizontal plane after installation, depending on the loading angle at the anchor chain (Gaudin et al., 2006). Liu et al. (2018a) investigated the influence of anchor inclination on the uplift bearing capacity and found that the capacity deceases with the increase of anchor inclination for fully bonded anchors. Moreover, the inclination has more influence on the uplift bearing capacity for shallowly buried anchors. In this study, the effect of anchor inclination is not examined and for simplicity, the anchor is assumed to be oriented horizontally. This assumption is consistent with the DNV design code for

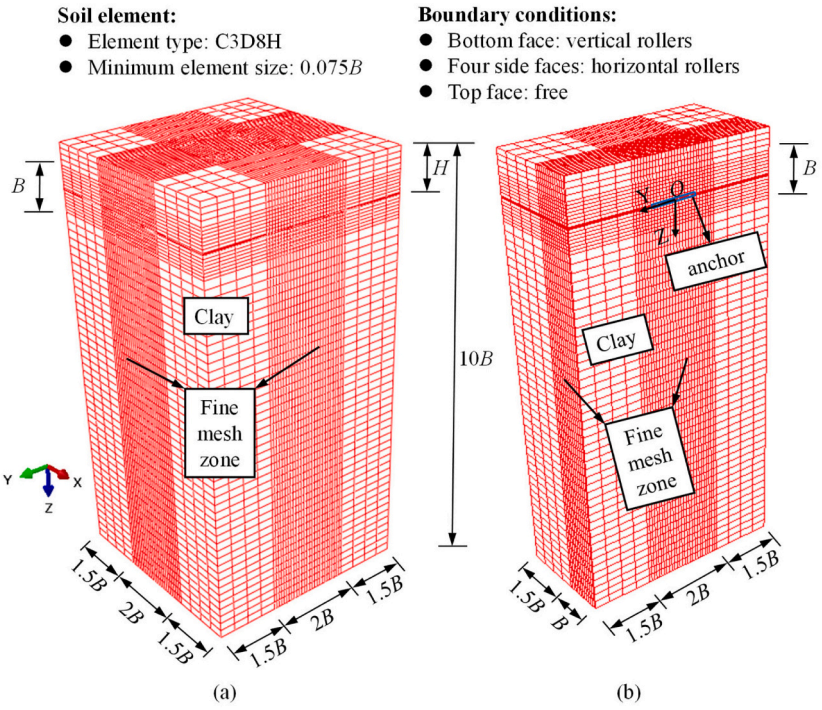

Fig. 3. 3D SSFE model of the square plate anchor and the soil domain: (a) whole model; (b) half model divided by YOZ plane. Note that the origin point "O" is defined as the center of the plate anchor.

Table 2
Finite element model parameters and soil properties.

Parameter	Symbol	Unit	Value
(a) Deterministic parameters			
Width of square plate anchor	B	m	4
Friction angle	φ	°	0
Undrained shear strength	s_{u0}	kPa	10
Dilation angle	ψ	°	0
Young's modulus	E	MPa	$500s_u$
Effective unit weight	γ'	kN/m^3	7
Initial geostatic stress factor	k_0	–	1.0
Minimum mesh size	h_{min}	m	0.075B
(b) Random field parameters			
Mean of undrained shear strength	u_{s_u}	kPa	10
Coefficient of variation	COV	–	0.3
Horizontal correlation length	Θ_H	m	20
Vertical correlation length	Θ_V	m	2

plate anchors (DNV, 2017).

In terms of meshing, a fine mesh zone with 2.0B in length, 2.0B in width and 1.0B in height is used for the soil domain in the vicinity of the plate anchor, as shown in Fig. 3. The 3D eight-node continuous hybrid element (C3D8H) and reduced-integration element (C3D8R) are adopted for the soil domain and the plate anchor, respectively. The minimum mesh size (h_{min}) is taken as 0.075B, which is small enough to ensure the computational accuracy (Wang et al., 2010). The contact between the anchor and the soil is assumed to be bonded, that is, no separation is allowed in the normal direction and the rough contact is assumed in the tangential direction. This fully bonded interface between the plate anchor and the soil could reasonably simulate an undrained condition (Li et al., 2015; Li et al., 2016). The normal restriction is applied to both the bottom and side walls of the soil domain.

The soil is modelled as an elastic-perfectly plastic material obeying a Mohr-Coulomb yield criterion. Both the friction angle (φ) and the dilatancy angle (ψ) are set to zero degrees to model the undrained saturated clay. The Poisson's ratio (ν) is set to be 0.49 to ensure an undrained analysis (Hu and Randolph, 1998; Chen et al., 2021a). As shown in Table 2, the undrained shear strength of clay is regarded as a random field parameter considering the geological uncertainty owing to the soil spatial variability. The Young's modulus (E) is also a random field parameter because it is considered as linearly correlated to the undrained shear strength (i.e., $E = 500s_u$). It is noted that the ultimate bearing capacity of a foundation is not significantly affected by changes in elastic parameters (Li et al., 2019). The effective unit weight (γ') of soil is taken as 7 kN/m^3. The geostatic step is performed first with an initial geostress factor of $k_0 = 1.0$ to balance the soil self-weight before uplift loading. The square plate anchor is treated as a rigid body with a reference point at the anchor centroid, as shown in Fig. 3(b). The whole anchor is displaced upward in the vertical direction at the reference point until a limiting uplift bearing capacity is attained. During uplift, translation and rotation movements of the anchor are restricted. This approach was adopted in order to examine the limiting vertical uplift bearing capacity. Note that, the results from additional SSFE analyses indicated that the effect of the anchor translation or rotation during uplift had limited effect on the uplift bearing capacity.

2.2. Spatially variable shear strength of soil

The effect of geological uncertainty such as spatially variable soil properties, on the geotechnical structures have been widely investigated since the most prestigious work done by Vanmarcke (1977). According to Phoon and Kulhawy (1999), the spatially variable soil property is often characterized via a mean value and a random residual value. This random component can be correlated in 3D space and governed by the autocorrelation function. The integral of the autocorrelation function results in the scale of fluctuation, within which the soil properties are strongly correlated (Li et al., 2015). In this study, we adopted the concept of scale of fluctuation. Due to the natural geological deposition process, the scale of fluctuation in the horizontal direction (Θ_H) is significantly greater than its counterpart in the vertical direction (Θ_V) (Phoon and Kulhawy, 1999; Li et al., 2016; Li et al., 2021). As for the

spatially variable undrained shear strength of clay, it is often assumed to be normally or log-normally distributed (Phoon et al., 2000; Cho, 2014; Zhu et al., 2015).

In this study, the spatial variable undrained shear strength is modelled as a log-normal random field. Following Yi et al. (2020) and Chen et al. (2021b), the mean (u_{su}) and COV of undrained shear strength are taken as 10 kPa and 0.3, respectively. The horizontal and vertical scales of fluctuation (Θ_H and Θ_V) are set to be 20 m and 2 m, respectively. The modified linear estimation method (Liu et al., 2014b) is firstly utilized to generate a 3D normal random field with a squared exponential auto-correlation function, according to the statistical parameters (u_{su}, COV, Θ_H and Θ_V). Then, the generated normal random field is exponentially transformed into a log-normal random field. The latter is finally mapped to the formerly established SSFE model using the user pre-defined field variable in ABAQUS (Dassault Systémes, 2018). The SSFE analysis on the uplift bearing capacity of a square plate anchor can then be realized in spatially variable soil. Fig. 4 depicts the undrained shear strength contours of a typical random soil sample. The red color represents relatively stronger soils while the blue color indicates weaker soils. The horizontal and vertical scales of fluctuation (Θ_H and Θ_V) are also marked in Fig. 4. As can be seen, the soil at a zone has a similar strength, which is obviously different from the strength in adjacent another zone. The size of the zone is governed by the scales of fluctuation.

3. Results and discussion

3.1. SSFE model validation

The established SSFE model is validated by comparison with the solutions from Wang et al. (2010), which reported the results of a horizontally wished-in-place square plate anchor at five varying buried depths (H = 0.5B, 1.0B, 2.0B, 3.0B, and 4.0B) in uniform soils. The comparison of uplift bearing capacity factors is shown in Fig. 5. As can be seen, the limiting uplift bearing capacity factors obtained in this study agree reasonably with those in Wang et al. (2010) for all buried depths. The biggest difference is only ~2.5% which occurs in the case of H/B = 0.5. When the normalized buried depth (H/B) exceeds ~2.0, the limiting uplift bearing capacity factor tends to be unchanged. It is noted that the results for H/B = 3.0 are not contained in Fig. 5(a) as they are the same as the solutions for H/B = 4.0. The relationship between the limiting bearing capacity factor and the buried depth can be well explained by the failure mechanisms of the soil surrounding the plate anchors.

Fig. 6 plots the soil displacement contours in the vicinity of the plate anchor at varying buried depths. For the shallowly buried anchor, the failure zone of soil extends to the ground surface, leading to the soil heave. As the buried depth increases from 0.5B to 1.0B, the plastic zone gradually expands, which results in an increase in the uplift bearing capacity factor from 11.43 to 13.68. When the buried depth exceeds 2.0B, the failure mode differs markedly from that of a shallowly buried plate anchor. In this case, the failure zone starts to exhibit a localized and symmetrical mode. With the increase of buried depth, the localized failure zone in Fig. 6(c–e) no longer enlarges and only translates into deeper soils, which leads to an almost unchanged limiting uplift bearing capacity factor of 14.13, as shown in Fig. 5(b). This behavior is consistent with that observed by Merifield et al. (2001) and Liu et al. (2018a).

3.2. Effect of soil non-homogeneity (kB/s_{u0})

Seabed clay is widely reported to have a linearly increasing undrained shear strength profile with soil depth (i.e., $s_{u0} = s_{um} + kz$), as stated before. To examine the effect of soil non-homogeneity (kB/s_{u0}) on the uplift bearing capacity of plate anchors, cases with four different shear strength gradients (k) of 0, 1.1, 2.2, and 3.3 kPa/m are considered following Liu et al. (2018a). The undrained shear strength at the mudline (s_{um}) is set as 2.4 kPa, and two representative buried depths (i.e., H = 1.0B and 4.0B) corresponding to shallowly and deeply buried scenarios are modelled, respectively. This leads to a soil non-homogeneity factor (kB/s_{u0}) ranging within 0 to 0.85 for H = 1.0B and 0 to 0.83 for H = 4.0B.

Table 3 shows the results of the uplift bearing capacity factor in the scenarios with different soil non-homogeneity factors. As can be seen, the uplift bearing capacity factor decreases with the increase of non-homogeneity factor. However, the magnitude of this decrease is relatively limited, which is less than ~3.6%. This is consistent with the result from Liu et al. (2018a), which reported that the soil non-homogeneity induced a 4% reduction in the uplift bearing capacity factor for a fully-bonded square plate anchor. Therefore, for the following study in spatially variable soil, the effect of soil non-homogeneity (kB/s_{u0}) will be neglected and the mean undrained shear strength of soil will be assumed as constant with soil depth (i.e., u_{su} = 10 kPa).

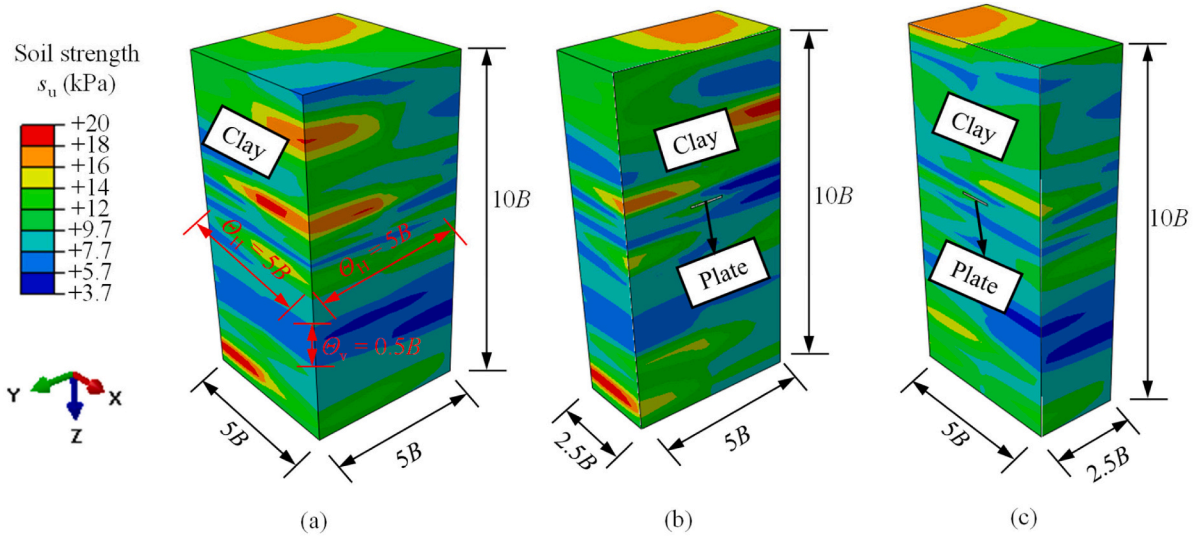

Fig. 4. Undrained shear strength contours from a typical 3D random soil sample: (a) full model; (b) half model divided by the YOZ-plane; (c) half model divided by the XOZ-plane (u_{s_u} = 10 kPa; Θ_H = 20 m; Θ_V = 2 m; COV = 0.3).

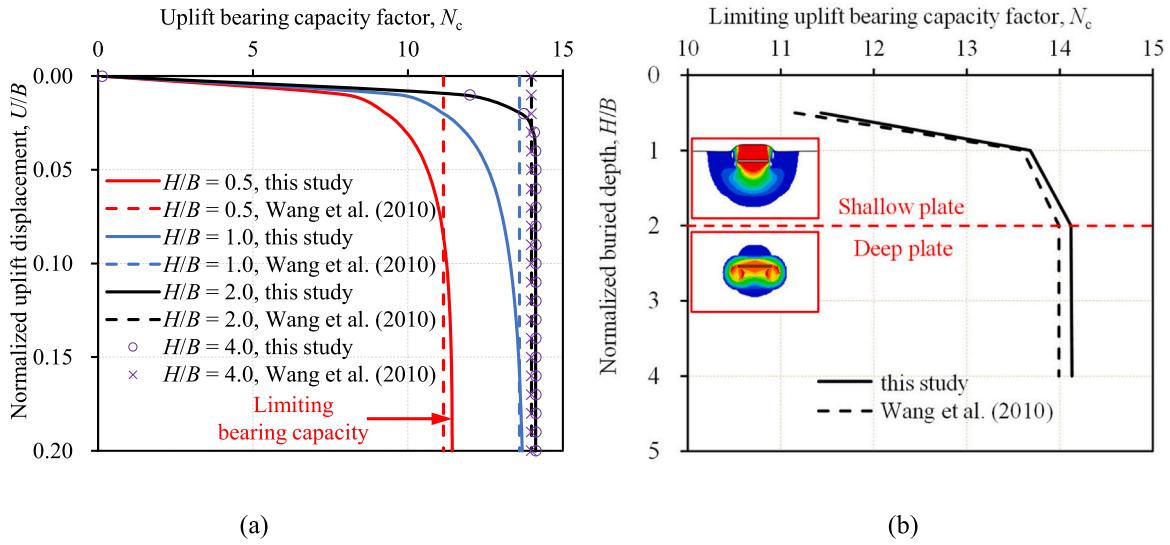

Fig. 5. Uplift bearing capacity factors of a square plate anchor at various buried depths in a uniform soil (s_{u0} = 10 kPa): (a) uplift bearing capacity factor vs normalized uplift displacement; (b) limiting uplift bearing capacity factor vs normalized buried depth. The failure mechanisms of shallowly and deeply buried plate anchors in a uniform soil are also noted in Fig. 5(b).

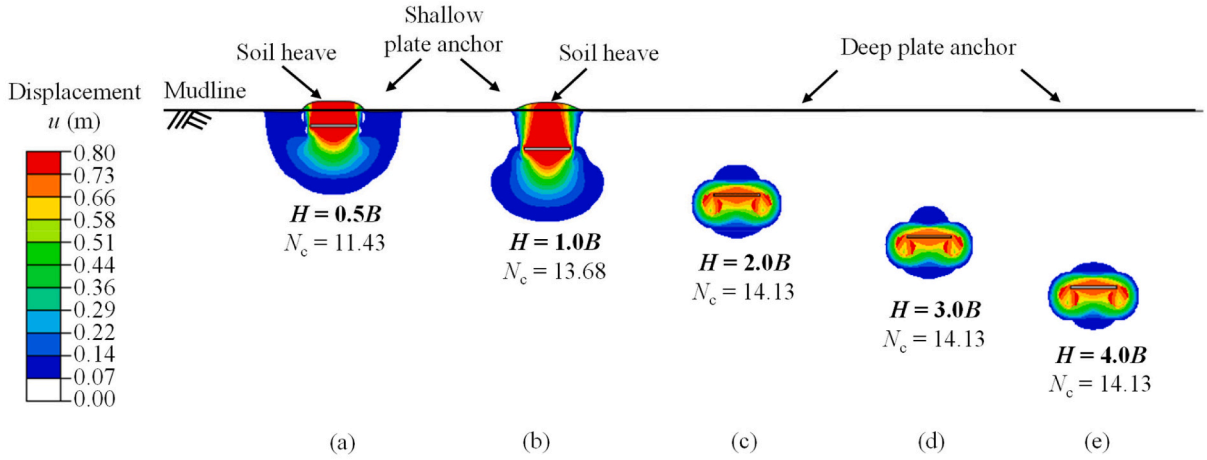

Fig. 6. Displacement fields plotted on YOZ-plane at five different buried depths (0.5B, 1.0B, 2.0B, 3.0B, and 4.0B) in a uniform soil (s_{u0} = 10 kPa): (a) H = 0.5B; (b) H = 1.0B; (c) H = 2.0B; (d) H = 3.0B; and (e) H = 4.0B.

Table 3
Effect of non-homogeneity factor on uplift bearing capacity factor.

H/B = 1	kB/s_{u0}	0	0.64	0.79	0.85
	N_c	13.68	13.46	13.28	13.19
H/B = 4	kB/s_{u0}	0	0.35	0.59	0.83
	N_c	14.13	14.04	14.03	14.03

3.3. Uplift bearing capacity factor in spatially variable soil

In uniform soils, the uplift bearing capacity factor of a plate anchor may be estimated via Eq. (1). Similarly, the uplift bearing capacity factor ($N_{c,ran}$) in spatially random soils can be calculated as below:

$$N_{c,ran} = \frac{Q_{u,ran}}{Au_{s_u}} \tag{3}$$

where $Q_{u,ran}$ is the uplift resistance of the plate anchor in spatially variable soils; u_{s_u} is the mean undrained shear strength of the random soil, which is assumed to be constant with soil depth and equals the deterministic value of s_{u0} = 10 kPa.

Fig. 7 shows the calculated uplift bearing capacity factors at five different buried depths (i.e., H = 0.5B, 1.0B, 2.0B, 3.0B, and 4.0B) in both uniform and spatially variable soils. Note that 100 repetitive Monte-Carlo simulations are performed for each buried depth in the random SSFE analyses. As can be seen, the calculated results for uniform soils in this study agree well with those reported in Wang et al. (2010). The uplift bearing capacity factor increases sharply at shallow normalized buried depth (H/B) of less than 2.0, and after that it tends to stabilize until reaching the limit value of N_c = 14.13. However, in spatially random soils, the uplift bearing capacity factor varies from one random soil sample to another with a fluctuation range between 6.0 and 21.0. This may be attributed to the various failure modes in different random scenarios, which will be discussed in the following section. Moreover, for each buried depth, the mean value of $N_{c,ran}$ in spatially random soil is generally lower than the counterpart in the uniform soil, indicating that the spatial variability of undrained shear strength will cause the reduction in the uplift bearing capacity factor of the plate anchor. For example, the mean value of $N_{c,ran}$ from the random analyses is 4.3%

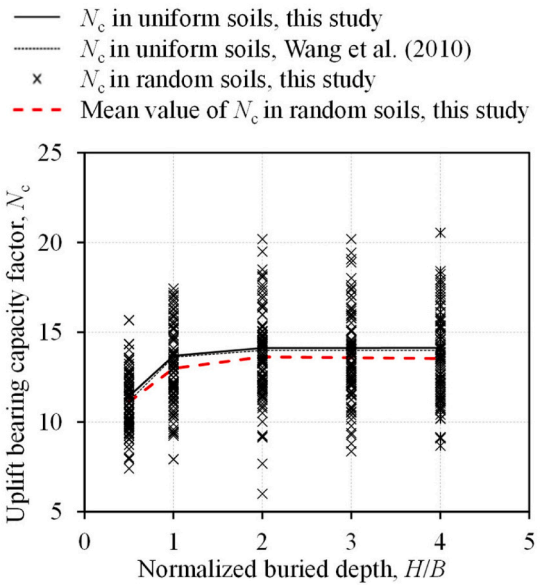

Fig. 7. Uplift bearing capacity factors (N_c) of square plate anchor with varying normalized buried depths (H/B) in both uniform and spatially random soils.

smaller than the deterministic value for a deeply buried plate anchor with $H/B = 4.0$. This phenomenon is similar to the random analyses for other geotechnical structures, such as slopes and tunnels (e.g., Ali et al., 2014; Huang et al., 2017; Jiang et al., 2020). This mechanism may be explained by the observation from Griffiths and Fenton (2001) that the shear failure would be more likely to propagate along weaker soil in spatially random soils. This reduction in the bearing capacity has also been observed in previous studies on the strip footings (Li et al., 2015) and plate anchors (Cai et al., 2022). The reduction of the mean $N_{c,ran}$ relative to the deterministic value in this study is essentially the same as the value (4%) observed by Cai et al. (2022) in 3D random SSFE analyses of a deep plate anchor. However, as reported by Li et al. (2015), the percentage of the reduction in the bearing capacity factor is approximately 9% for the strip footing under 2D plane strain conditions, which is higher than the results obtained in this study and Cai et al. (2022). This is expected to be the fact that the finite scale of fluctuation in the longitudinal direction of the plate anchor permits some degree of out-of-plane averaging in the 3D analyses. This reduces the chance of the 3D anchor finding a weaker soil zone and enhances the spatial averaging effect in the undrained shear strength (Cai et al., 2022). As the scale of fluctuation in the longitudinal direction of plate anchor increases, the effect of out-of-plane averaging becomes less effective, and the 3D results approach the 2D counterparts (Pan et al., 2021).

Fig. 8 shows the distributions of the uplift bearing capacity factor at five different buried depths in spatially random soils. The Kolmogorov-Smirnov (K—S) normal distribution goodness-of-fit test is performed to fit the calculated data. As can be seen, the D_{max} values, defined as the maximum difference of the cumulative probability between the sample and the reference distribution, in all cases are less than the critical K-S test statistic D_0, which is 0.136 at 5% significance level for a sample with 100 data points. Hence, the $N_{c,ran}$ in this study can be treated as normally distributed in the following. The results of the mean and COV of $N_{c,ran}$ based on the Monte-Carlo simulations are presented in Table 4 and Fig. 9. It can be observed from Fig. 9 that 100 Monte-Carlo simulations are sufficient to give a reliable statistical solution.

It can be also observed from Table 4 that the COV of the uplift bearing capacity factor, which fluctuates from 0.15 to 0.18, is always smaller than the COV of the undrained shear strength (i.e., 0.3). This is owing to the spatial averaging of the shear strength of the mobilized soil. The uplift bearing capacity in random soils is influenced by the averaging effect of the undrained shear strength of the soil in the failure zone, which leads to the variability of the uplift bearing capacity factor being smaller than that of the soil strength itself. For a deep plate anchor in this study, the COV of $N_{c,ran}$ is around 50–60% of the COV of s_u, owing to the local spatial averaging effect. However, in the problem of strip footings, Li et al. (2015) reported that the COV of the bearing capacity factor is only 20% of the COV of s_u for a deeply buried strip footing. This difference may be explained by the relatively smaller scales of fluctuation ($\Theta_H/B = 2.5$; $\Theta_V/B = 0.19$) used in Li et al. (2015). Note that the values of Θ_H/B and Θ_V/B used in this study are 5 and 0.5. Cai et al. (2022) investigated the effect of the scale of fluctuation on the uplift bearing capacity factor and found that the COV of the uplift bearing capacity factor rises significantly with the increase in Θ_H/B and Θ_V/B. When Θ_H/B is large enough (e.g., $\Theta_H/B = 100$), there is almost no spatial averaging of the soil strength since the strength of the mobilized soil influencing the uplift bearing capacity of the anchor is essentially uniform. Therefore, in this case the COV of $N_{c,ran}$ is expected to equal the COV of s_u (Cai et al., 2022).

3.4. Failure mechanisms in spatially random soils

Fig. 10 shows the displacement fields and undrained shear strength contours of the soil surrounding a square plate anchor with a shallowly buried depth of $H = 0.5B$ in the uniform soil and three typical random soil samples (Nos. 12, 30, and 59, corresponding to the moderate, maximum, and minimum uplift bearing capacity factors, respectively). Similar to the aforementioned finding, the failure zones for the shallowly buried cases ($H = 0.5B$) extend to the ground surface in both uniform and spatially random soils. The displacement field of the soil surrounding the anchor exhibits a symmetrical failure mode in the deterministic soil while it is asymmetrical and irregular in the random samples, which may be attributed to the corresponding undrained shear strength of the soil.

As the spatial variability in the undrained shear strength increases, the corresponding failure mode deviates from the deterministic failure mode. For example, in the random soil sample of No. 59 in Fig. 10(h), relatively weaker soil with a lower undrained shear strength of approximately 2 kPa surrounds the plate anchor, which results in a smaller failure zone of soil in Fig. 10(d), when compared to the uniform case in Fig. 10(a). This is because the shear band tends to develop along the weaker soil. As a result, the corresponding uplift bearing capacity factor of the anchor in this case is only 7.39, which is smaller than the deterministic value of 11.43. In contrast, for the soil sample of No. 30, the stronger soil ($s_u \approx 18$ kPa) is evenly distributed around the anchor. This makes the shear failure band develop downward, which forms a larger plastic failure zone in Fig. 10(c). The combined effects of the larger failure zone and the stronger soil inside the zone result in a larger uplift bearing capacity factor of 15.67. Conversely, the soil strength around the anchor in the sample of No. 12 is relatively close to that of the uniform soil, which expectedly leads to a similar failure mechanism and hence an equivalent uplift bearing capacity factor of 11.43.

Figs. (11–14) show the results of soil displacement fields and undrained shear strength contours for the plate anchor with buried depths of $H = 1.0B$, $2.0B$, $3.0B$, $4.0B$ in the uniform soil and three random soil samples, respectively. Similar to that observed before, the failure mechanism in the spatially random soil is typically dictated by the buried depth, but it will change to some extent when the surrounding random soil is stronger or weaker than the uniform soil. For example, in Fig. 11, the failure mode for the scenario with a buried depth of $H = 1.0B$ typically exhibits a global failure mechanism and extends to the ground surface, however, in the random case with weak soil strength surrounding the plate anchor, i.e., Random sample of No. 36, it no longer extends to the ground surface but rather shows a localized rotational scoop failure mode, which often occurs in the scenarios with deeper buried depths. The change from a global shear failure to a localized rotational failure reduces the uplift bearing capacity from 13.68 for the

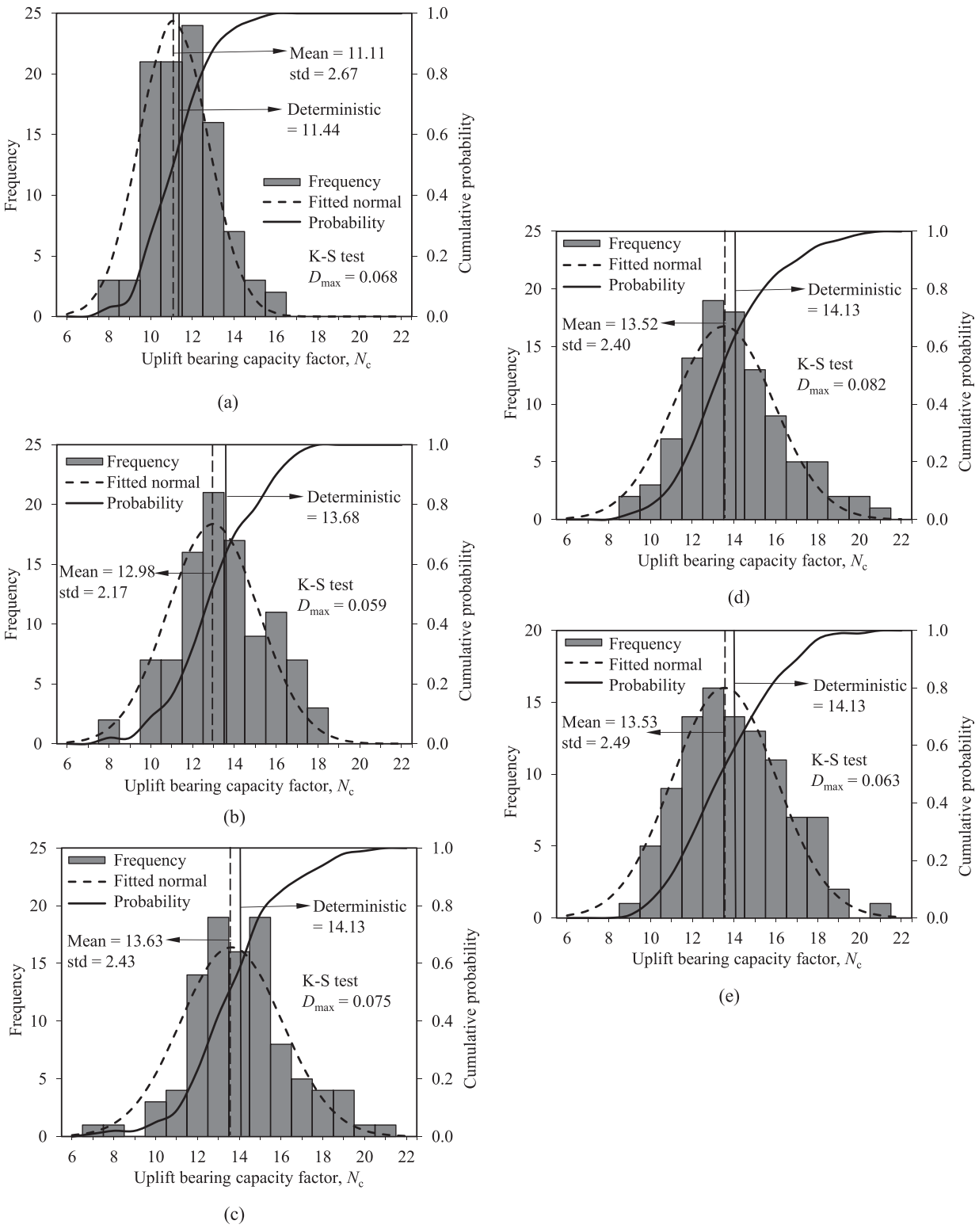

Fig. 8. Histograms of uplift bearing capacity factors at five different buried depths: (a) $H = 0.5B$; (b) $H = 1.0B$; (c) $H = 2.0B$; (d) $H = 3.0B$; (e) $H = 4.0B$.

uniform soil to 7.91 for the random sample of No. 36. Likewise, for the scenarios with a buried depth $H = 2.0B$ in Fig. 12, the case with strong random soil strength (i.e., Random No. 93) shows a global failure mode. This indicates that the weak and strong random soil strengths around the anchor may contribute to forming a localized rotational scoop failure mechanism and a global shear failure mechanism, respectively. The buried depth of $H = 2.0B$ cannot serve as a critical value to ensure a localized failure mechanism in spatially random soils since the ground may heave under this circumstance. In terms of the uplift bearing capacity factor, the strong random soil strength greatly increases the uplift bearing capacity factor while the weak soil strength acts oppositely.

For ultimately deep plate anchors ($H = 3.0B$ and $4.0B$) in Figs. 13 and 14, only local failure modes are observed and the plastic failure zone no longer extends to the ground surface in both uniform and spatially

Table 4
Statistic parameters of the uplift bearing capacity factor (Monte-Carlo simulation No. = 100).

Buried depth H	Deterministic value N_c	Mean $u_{Nc,ran}$	Standard deviation $\sigma_{Nc,ran}$	COV $\sigma_{Nc,ran}$
0.5B	11.44	11.11	1.64	0.15
1.0B	13.68	12.98	2.17	0.17
2.0B	14.13	13.63	2.43	0.18
3.0B	14.13	13.52	2.40	0.18
4.0B	14.13	13.53	2.49	0.18

random soils. This implies that a buried depth of $H = 3.0B$ is sufficient to ensure a localized failure mechanism in spatially random soils, while with $H = 2.0B$ a localized failure mechanism is ensured in uniform soil only. Therefore, the spatial variability of undrained shear strength tends to increase the critical buried depth at which a global shear failure evolves into a localized rotational scoop failure. Note that Li et al. (2015) also reported a transition depth of 3.0B to achieve a localized failure mechanism for a strip footing in spatially variable soil, which is in good agreement with this research finding.

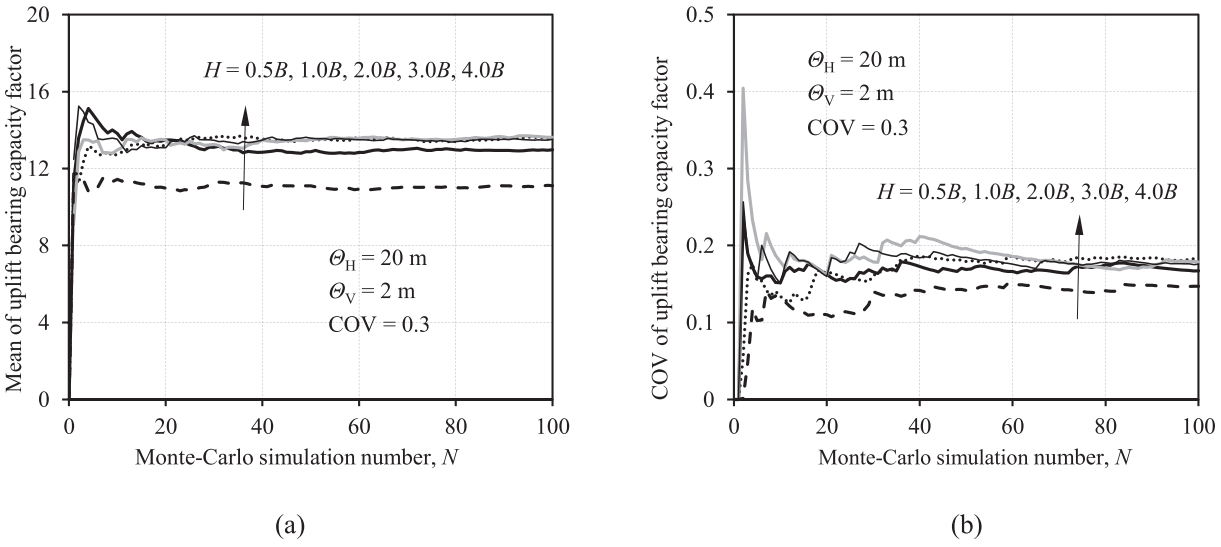

Fig. 9. The evolution of the mean and COV of uplift bearing capacity factors with Monte-Carlo simulation number: (a) mean value; (b) COV.

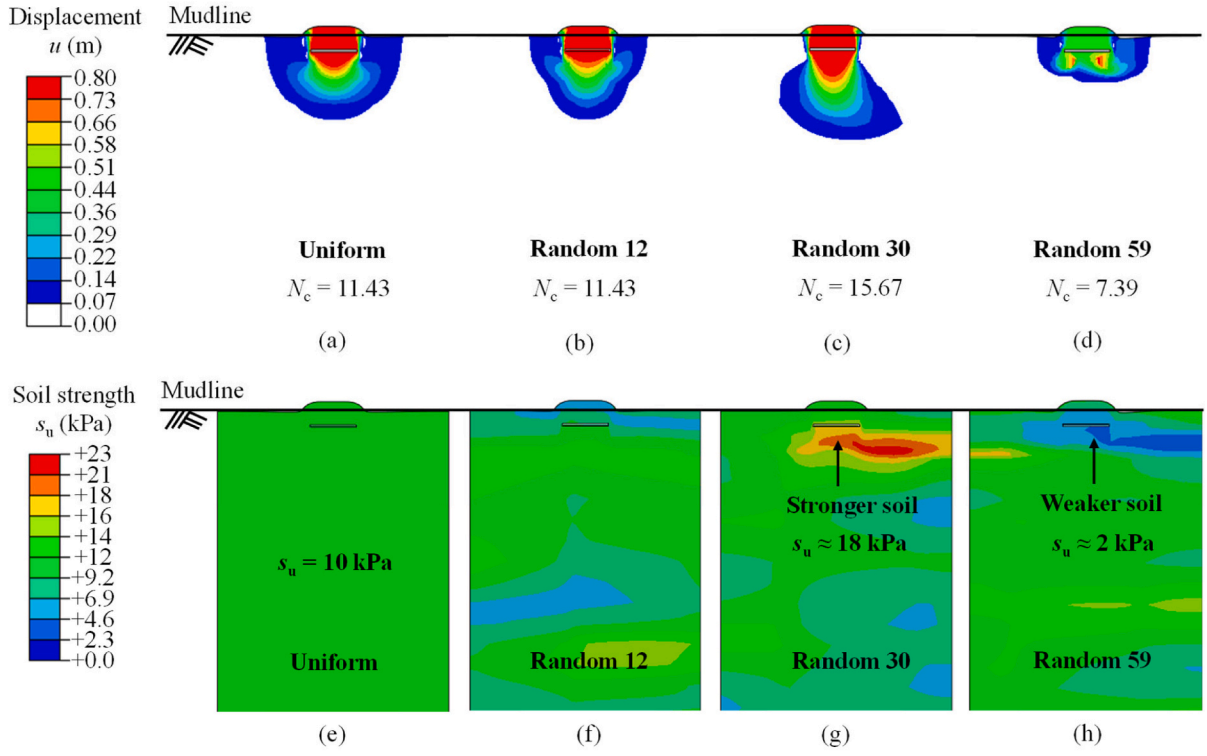

Fig. 10. Displacement fields and undrained shear strength contours of soil surrounding a square plate anchor with a buried depth of $H = 0.5B$ in the uniform soil and three random soil samples (i.e., Nos. 12, 30 and 59): (a–d) displacement fields of soil; (e–h) undrained shear strength contours of soil.

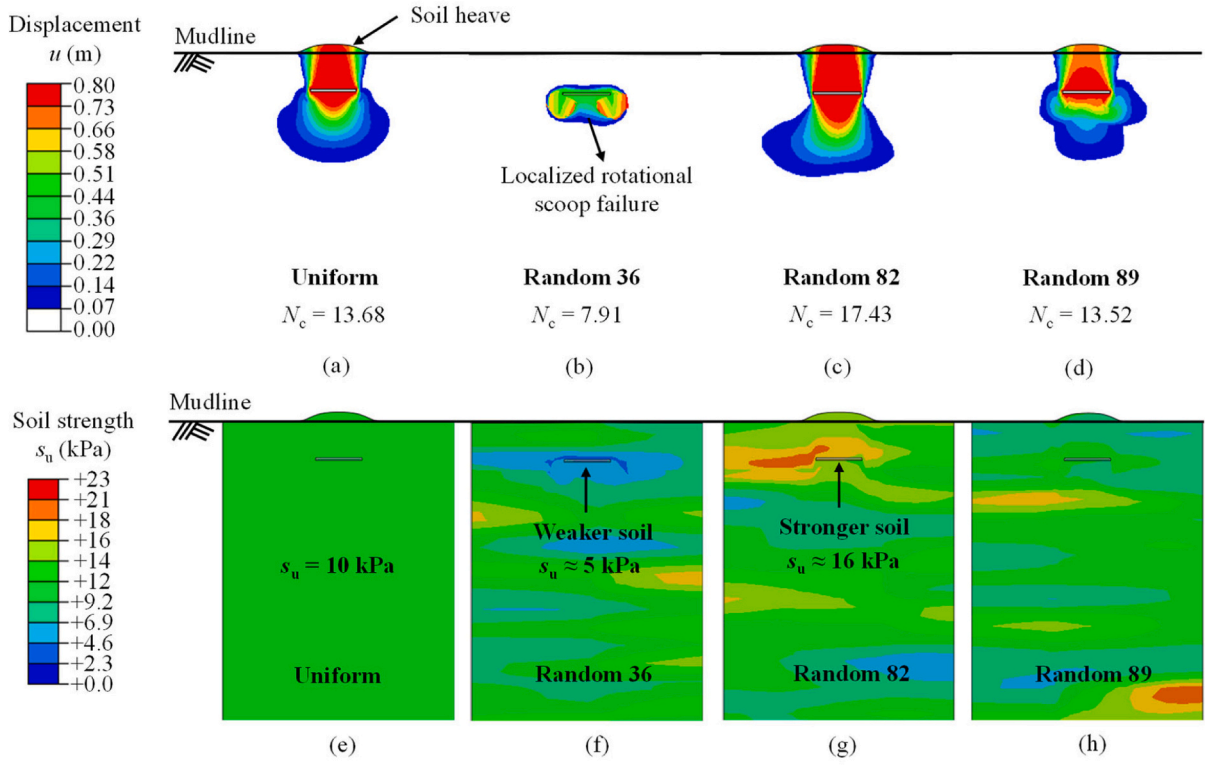

Fig. 11. Displacement fields and undrained shear strength contours of soil surrounding a square plate anchor with a buried depth of $H = 1.0B$ in the uniform soil and three random soil samples (i.e., Nos. 36, 82 and 89): (a–d) displacement fields of soil; (e–h) undrained shear strength contours of soil.

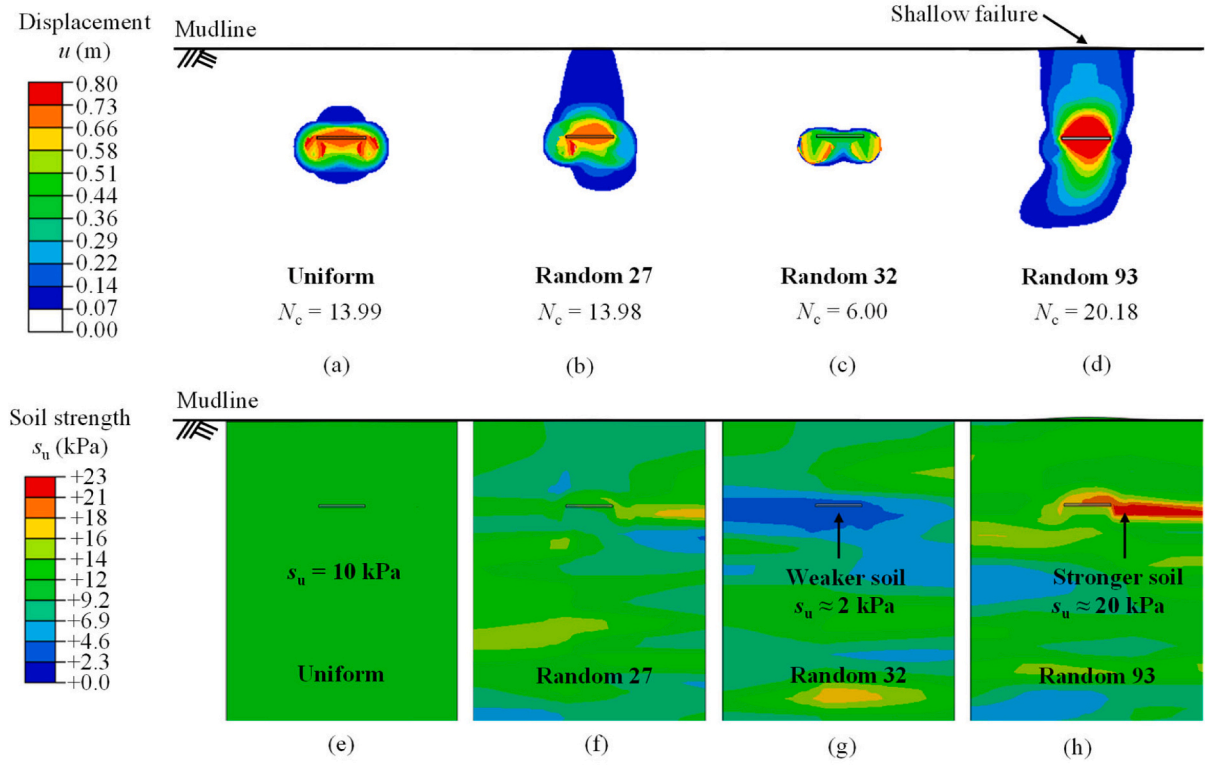

Fig. 12. Displacement fields and undrained shear strength contours of soil surrounding a square plate anchor with a buried depth of $H = 2.0B$ in the uniform soil and three random soil samples (i.e., Nos. 27, 32 and 93): (a–d) displacement fields of soil; (e–h) undrained shear strength contours of soil.

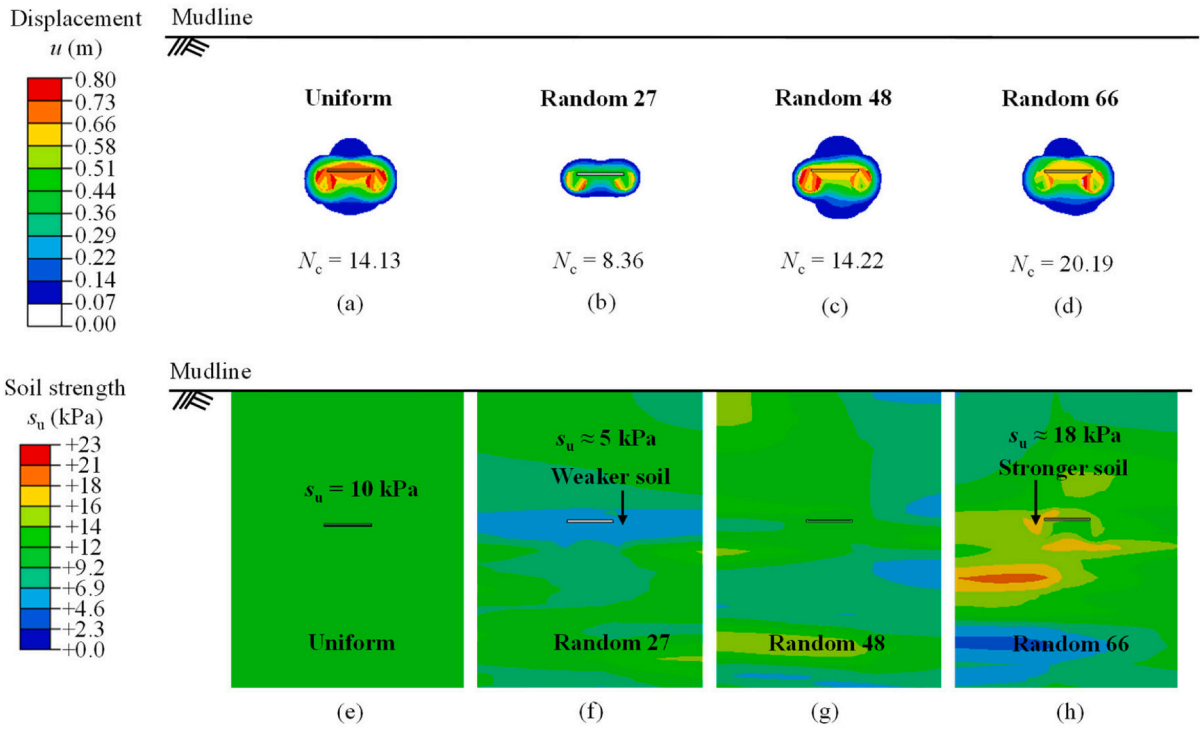

Fig. 13. Displacement fields and undrained shear strength contours of soil surrounding a square plate anchor with a buried depth of $H = 3.0B$ in the uniform soil and three random soil samples (i.e., Nos. 27, 48 and 66): (a–d) displacement fields of soil; (e–h) undrained shear strength contours of soil.

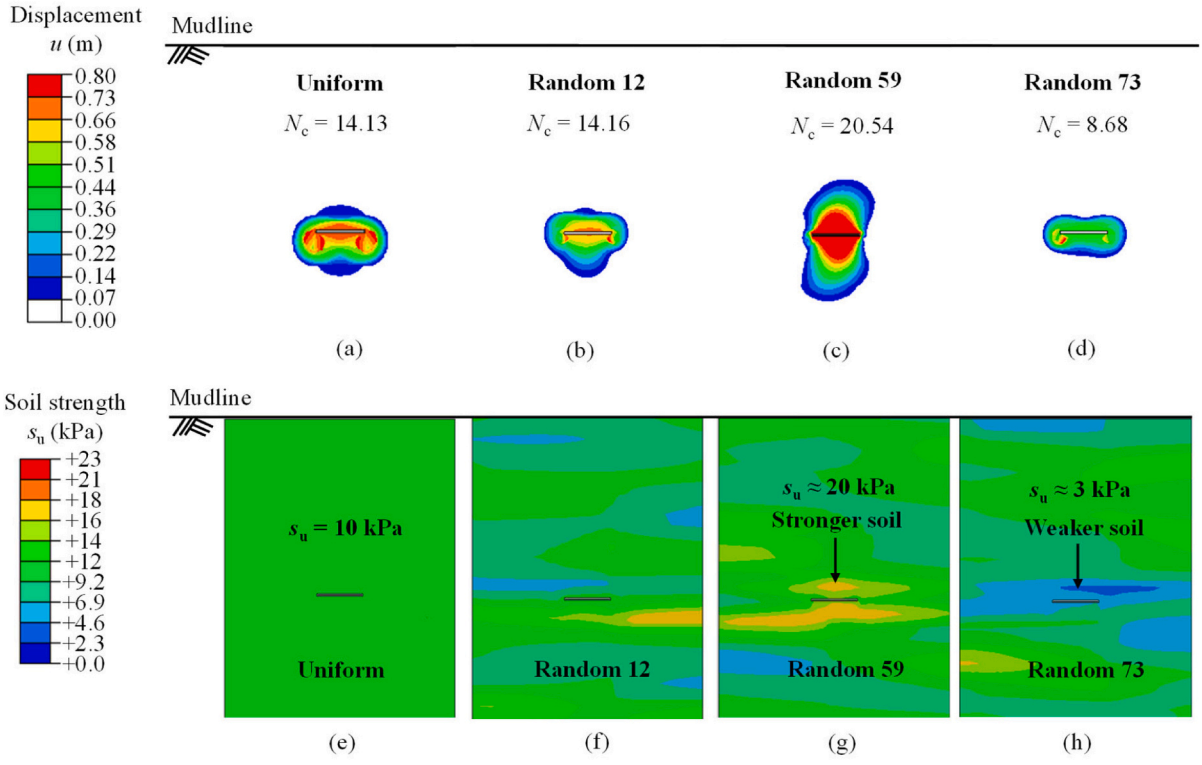

Fig. 14. Displacement fields and undrained shear strength contours of soil surrounding a square plate anchor with a buried depth of $H = 4.0B$ in the uniform soil and three random soil samples (i.e., Nos. 12, 59 and 73): (a–d) displacement fields of soil; (e–h) undrained shear strength contours of soil.

3.5. Probability of failure in spatially random soil

The factor of safety (FOS) approach is commonly used in the assessment of foundation stability. In accordance with Li et al. (2015), the FOS approach is introduced into this study to account for the reduction of anchor uplift bearing capacity in spatially random soils ($N_{c,ran}$) relative to that in uniform soils (N_c). Based on this approach, the probability of failure for a square plate anchor with a normally distributed uplift bearing capacity factor ($N_{c,ran}$) can be expressed as:

$$P\left(N_{c,ran} < N_c/\mathrm{FOS}\right) = \boldsymbol{\Phi}\left[\frac{N_c/\mathrm{FOS} - \mu_{N_{c,ran}}}{\sigma_{N_{c,ran}}}\right] \quad (4)$$

where Φ is the cumulative normal function; $\mu_{N_{c,\ ran}}$ and $\sigma_{N_{c,\ ran}}$ are the mean value and standard deviation of $N_{c,ran}$, respectively, (listed in Table 4). Thus, based on Eq. (4), the probability of failure can be directly corelated to the FOS.

Table 5 shows the relationship between the probability of failure and the FOS of a square plate anchor at five different buried depths. As can be seen, the square plate anchor has a considerable probability of failure when the FOS = 1.0. This is because the mean value of $N_{c,ran}$ for a random soil is generally less than the value of N_c derived from the deterministic soil, as shown in Table 4. However, the probability of failure decreases dramatically with the increase of the FOS from 1.0 to 1.3. After that, the probability of failure gradually reduces to zero as the FOS approaches 1.9. According to Li et al. (2015), the probability of failure within 10^{-2} to 10^{-4} is required to provide a reliable design for a foundation. Table 6 shows the results of the FOS with the probability of failure ranging from 10^{-2} to 10^{-4}. As can be seen, a FOS of 1.9 is sufficient to limit the probability of failure to below 1%.

DNV (2017) recommended a partial safety factor of 1.4 for the buried plate anchor at ultimate limit state to account for the uncertainty in undrained shear strength of soil material adopted for design. As shown in Table 5, this material factor corresponds to the probability of failure of 3.7%, 7.0%, 7.3%, 7.5%, and 8.4% for the plate anchor buried at 0.5B, 1.0B, 2.0B, 3.0B, and 4.0B, which indicates this partial safety factor of 1.4 recommended by DNV (2017) seems insufficient to ensure the safety design of plate anchors. However, DNV (2017) also listed the partial safety (load) factors of 1.1 for the mean load component and 1.5 for the dynamic load component to reflect the uncertainty in the design loads. In accordance with the basis of limit state design, these partial material and load factors must be used together and not in isolation for foundation design. Consider a hypothetical scenario where a design load comprises the mean and dynamic load components. In this case a hybrid partial load factor of 1.3 (the average of 1.1 and 1.5) can be adopted. We can then consider a global (lumped) design FOS of 1.82 equal to the product of the partial material factor (1.4) and the partial load factor (1.3). Interestingly, this value is broadly similar to the value of 1.9 inferred by this research finding as being sufficient to ensure a probability of failure below 1%.

Furthermore, the results in Table 5 also demonstrates that the deeply buried anchor generally has a larger probability of failure, owing to a larger COV of the uplift bearing capacity factor at the deep embedment (see Table 4). As a result, a larger FOS is required to achieve a target probability of failure in Table. 6.

Table 5
Probability of failure (%) with varying FOSs at five different buried depths.

FOS	Probability of failure (%)				
	Buried depth, H				
	0.5B	1.0B	2.0B	3.0B	4.0B
1.0	57.97	62.65	58.15	59.87	59.52
1.3	7.95	12.88	12.80	13.38	14.26
1.4	3.66	6.96	7.28	7.50	8.37
1.8	0.19	0.66	0.87	0.90	1.13
2.0	0.05	0.23	0.34	0.35	0.47
2.5	0.00	0.03	0.05	0.06	0.08

Table 6
FOS values with varying probability of failure (%) at five different buried depths.

Probability of failure: %	FOS				
	Buried depth, H				
	0.5B	1.0B	2.0B	3.0B	4.0B
1	1.57	1.72	1.77	1.78	1.83
0.1	1.89	2.18	2.31	2.32	2.42
0.01	2.28	2.79	3.04	3.05	3.07

4. Conclusions

This study conducted 3D random SSFE analyses to investigate the uplift bearing capacity and failure mechanisms of a square plate anchor buried at different depths considering the geological uncertainty owing to the soil spatial variability. The established SSFE model was first validated by comparing the uplift bearing capacity with previous solutions in uniform soils. Then, the combined effects of anchor buried depth and soil spatial variability on the uplift bearing capacity and failure mechanism were investigated in detail. The main findings are summarized as follows:

(1) In random soils, the plastic failure zone of soil surrounding the square plate anchor typically exhibits asymmetrical and irregular distributions. Two typical types of failure mechanisms, namely a localized rotational scoop failure mechanism and a global shear failure mechanism would form in random soils with relatively weak and strong soil strengths, respectively. A larger buried depth of 3.0B (B = width of plate anchor) is required to ensure a localized failure mode in spatially random soils.
(2) The computed uplift bearing capacity factor ($N_{c,ran}$) in random soils varies in a relatively wide range. The mean uplift bearing capacity in random soil is generally lower than the corresponding deterministic value. For this reason, the deterministic uplift bearing capacity is always overestimated.
(3) The probability of failure for square plate anchors in spatially random soil is corelated to the conventional FOS. Based on this, a quantitative approach is provided to predict the probability of failure for plate anchors considering the combined effects of anchor buried depth and soil spatial variability, which may benefit the estimation of probability of failure for square plate anchors in the conventional FOS-based design.

In the current SSFE analyses, the probability of failure was evaluated based on a spatially variable soil with particular strength and strength variability parameters (u_{s_u} = 10 kPa; COV = 0.3; Θ_H = 20 m; Θ_V = 2 m). More numerical simulations should be conducted to explore the effects of the scales of fluctuation and COV on the uplift bearing capacity and probability of failure for square plate anchors in the follow-up study.

CRediT authorship contribution statement

Xue-Jian Chen: Methodology, Software, Investigation, Visualization, Writing – original draft, Writing – review & editing. **Yong Fu:** Methodology, Investigation, Writing – original draft, Writing – review & editing. **Yong Liu:** Conceptualization, Investigation, Writing – review & editing.

Declaration of Competing Interest

The authors declare that they have no known competing financial interests or personal relationships that could have appeared to influence

the work reported in this paper.

Acknowledgements

This research is supported by the National Natural Science Foundation of China (Grant Nos. 52079099, 52001157).

Notation

A	Base area of square plate anchor
B	Width of square plate anchor
D_{max}	Maximum difference of cumulative probability for the sample and the reference distribution
E	Young's modulus
Q_u	Uplift resistance of square plate anchor in deterministic soil
$Q_{u,ran}$	Uplift resistance of square plate anchor in spatially random soil
H	Buried depth of square plate anchor
h_{min}	Minimum mesh size used in finite element model
k	Gradient of undrained shear strength
k_0	Initial geostatic stress factor
N	Number of Monte Carlo simulations
N_c	Uplift bearing capacity factor in deterministic soil
$N_{c,ran}$	Uplift bearing capacity factor in spatially random soil
p	Probability of failure for square plate anchor
s_u	Undrained shear strength of random soil
s_{u0}	Undrained shear strength at the plate centroid for deterministic soil
s_{um}	Undrained shear strength at mudline level for deterministic soil
t	Thickness of square plate anchor
U	Uplift displacement of square plate anchor in soil
z	Depth of soil layer
γ'	Submerged unit weight of soil
φ	Friction angle of soil
ψ	Dilatancy angle of soil
β	Anchor inclination angle
ν	Poisson's ratio
u_{s_u}	Mean undrained shear strength in spatially variable soil
$\mu_{N_{c,ran}}$	Mean value of uplift bearing capacity factors in spatially random soil
$\sigma_{N_{c,ran}}$	Standard deviation of uplift bearing capacity factors in spatially random soil
Θ_H	Horizontal scale of fluctuation
Θ_V	Vertical scale of fluctuation
Φ	Cumulative normal function
2D	Two-dimensional
3D	Three-dimensional
COV	Coefficient of variation
COV_{N_c}	Coefficient of variation of uplift bearing capacity factors in spatially random soil
CEL	Coupled Eulerian-Lagrangian
FOS	Factor of safety
LB	Lower bound analysis
UB	Upper bound analysis
LFDE	Large deformation finite element
RITSS	Remeshing and interpolation technique with small strain
SEPLA	Suction embedded plate anchor
SSFE	Small strain finite element
VLA	Vertically loaded anchor

References

Ali, A., Huang, J., Lyamin, A.V., Sloan, S.W., Griffiths, D.V., Cassidy, M.J., Li, J.H., 2014. Simplified quantitative risk assessment of rainfall-induced landslides modelled by infinite slopes. Eng. Geol. 179, 102–116.

Cai, Y., Bransby, M.F., Gaudin, C., Tian, Y., 2022. Accounting for soil spatial variability in plate anchor design. J. Geotech. Geoenviron. 148 (2), 04021178.

Cassidy, M., Uzielli, M., Tian, Y., 2013. Probabilistic combined loading failure envelopes of a strip footing on spatially variable soil. Comput. Geotech. 49, 191–205.

Chen, X., Han, C., Liu, J., Hu, Y., 2021a. Interpreting strength parameters of strain-softening clay from shallow to deep embedment using ball and T-bar penetrometers. Comput. Geotech. 138, 104331.

Chen, X., Li, D., Tang, X., Liu, Y., 2021b. A three-dimensional large-deformation random finite-element study of landslide runout considering spatially varying soil. Landslides 18, 3149–3162.

Chen, Z., Tho, K.K., Leung, C.F., Chow, Y.K., 2013. Influence of overburden pressure and soil rigidity on uplift behavior of square plate anchor in uniform clay. Comput. Geotech. 52, 71–81.

Cho, S.E., 2014. Probabilistic stability analysis of rainfall-induced landslides considering spatial variability of permeability. Eng. Geol. 171, 11–20.

Das, B.M., 1978. Model tests for uplift capacity of foundations in clay. Soils Found. 18 (2), 17–24.

Das, B.M., 1980. A procedure for estimation of ultimate uplift capacity of foundations in clay. Soils Found. 20 (1), 77–82.

Das, B.M., Puri, V.K., 1989. Holding capacity of inclined square plate anchors in clay. Soils Found. 29 (3), 138–144.

Das, B.M., Moreno, R., Dallo, K.F., 1985. Ultimate pullout capacity of shallow vertical anchors in clay. Soils Found. 25 (2), 148–152.

Dassault Systémes, 2018. Analysis user's Manual, Version 2018. SIMULIA, Providence, RI.

DNV, 2017. Design and installation of plate anchors in clay. In: Recommended Practice DNV-RP-E302. Det Norske Veritas.

Evans, T.M., Zhang, N., 2019. Three-dimensional simulations of plate anchor pullout in granular materials. Int. J. Geomech. 19 (4), 04019004.

Feng, T., Zong, J., Jiang, W., Zhang, J., Song, J., 2020. Ultimate pullout capacity of a square plate anchor in clay with an interbedded stiff Layer. Advan. Civil Eng. 2020 https://doi.org/10.1155/2020/8867678.

Gaudin, C., O'loughlin, C.D., Randolph, M.F., Lowmass, A.C., 2006. Influence of the installation process on the performance of suction embedded plate anchors. Géotechnique 56 (6), 381–391.

Griffiths, D.V., Fenton, G.A., 2001. Bearing capacity of spatially random soil: the undrained clay Prandtl problem revisited. Géotechnique 51 (4), 351–359.

Griffiths, D.V., Fenton, G.A., Manoharan, N., 2002. Bearing capacity of rough rigid strip footing on cohesive soil: probabilistic study. J. Geotech. Geoenviron. 128 (9), 743–755.

Hu, Y., Randolph, M.F., 1998. Deep penetration of shallow foundations on non-homogeneous soil. Soils Found. 38 (1), 241–246.

Huang, H.W., Xiao, L., Zhang, D.M., Zhang, J., 2017. Influence of spatial variability of soil Young's modulus on tunnel convergence in soft soils. Eng. Geol. 228, 357–370.

Jiang, S.H., Li, D.Q., Zhang, L.M., Zhou, C.B., 2014. Slope reliability analysis considering spatially variable shear strength parameters using a non-intrusive stochastic finite element method. Eng. Geol. 168, 120–128.

Jiang, S.H., Huang, J., Qi, X.H., Zhou, C.B., 2020. Efficient probabilistic back analysis of spatially varying soil parameters for slope reliability assessment. Eng. Geol. 271, 105597.

Li, D.Q., Ding, Y.N., Tang, X.S., Liu, Y., 2021. Probabilistic risk assessment of landslide-induced surges considering the spatial variability of soils. Eng. Geol. 283, 105976.

Li, J.H., Tian, Y.H., Cassidy, M.J., 2015. Failure mechanism and bearing capacity of footings buried at various depths in spatially random soil. J. Geotech. Geoenviron. 141 (2), 04014099.

Li, J.H., Zhou, Y., Zhang, L.L., Tian, Y., Cassidy, M.J., Zhang, L.M., 2016. Random finite element method for spudcan foundations in spatially variable soils. Eng. Geol. 205, 146–155.

Li, Y.J., Liu, K., Zhang, B., Xu, N.X., 2019. Reliability of shape factors for bearing capacity of square footings on spatially varying cohesive soils. Int. J. Geomech. 20 (3), 04019195.

Liu, H.X., Su, F.M., Li, Z., 2014a. The criterion for determining the ultimate pullout capacity of plate anchors in clay by numerical analysis. Am. J. Eng. Appl. Sci. 7 (4), 374–386.

Liu, J., Tan, M.X., Hu, Y., 2018a. New analytical formulas to estimate the pullout capacity factor for rectangular plate anchors in NC clay. Appl. Ocean Res. 75, 234–247.

Liu, Y., Lee, F.H., Quek, S.T., Beer, M., 2014b. Modified linear estimation method for generating multi-dimensional multivariate Gaussian field in modelling material properties. Probabilistic Eng. Mech. 38, 42–53.

Liu, Y., Zhang, W.G., Zhang, L., Zhu, Z.R., Hu, J., Wei, H., 2018b. Probabilistic stability analyses of undrained slopes by 3D random fields and finite element methods. Geosci. Front. 9 (6), 1657–1664.

Merifield, R.S., Sloan, S.W., Yu, H.S., 2001. Stability of plate anchors in undrained clay. Géotechnique 51 (2), 141–153.

Merifield, R.S., Lyamin, A.V., Sloan, S.W., 2003. Three-Dimensional lower bound solutions for stability of plate anchors in clay. J. Geotech. Geoenviron. 129 (3), 243–253.

Merifield, R.S., Lyamin, A.V., Sloan, S.W., 2005. Stability of inclined strip anchors in purely cohesive soil. J. Geotech. Geoenviron. 131 (6), 792–799.

O'Neill, M.P., Bransby, M.F., Randolph, M.F., 2003. Drag anchor fluke soil interaction in clays. Can. Geotech. J. 40 (1), 78–94.

Pan, Y., Liu, Y., Tyagi, A., Lee, F.H., Li, D.Q., 2021. Model-independent strength-reduction factor for effect of spatial variability on tunnel with improved soil surrounds. Géotechnique 71 (5), 406–422.

Phoon, K.K., Kulhawy, F.H., 1999. Characterization of geotechnical variability. Can. Geotech. J. 36 (4), 612–624.

Phoon, K.K., Kulhawy, F.H., Grigoriu, M., 2000. Reliability-based design for transmission line structure foundations. Comput. Geotech. 26, 169–185.

Randolph, M.F., Gaudin, C., Gourvenec, S.M., White, D.J., Boylan, N., Cassidy, M.J., 2011. Recent advances in offshore geotechnics for deep water oil and gas developments. Ocean Eng. 38 (7), 818–834.

Rowe, R.K., Davis, E.H., 1982. The behaviour of anchor plates in clay. Geotechnique 32 (1), 9–23.

Song, Z., Hu, Y., Randolph, M.F., 2008. Numerical simulation of vertical pullout of plate anchors in clay. J. Geotech. Geoenviron. 134 (6), 866–875.

Srivastava, A., Babu, G.S., 2009. Effect of soil variability on the bearing capacity of clay and in slope stability problems. Eng. Geol. 108, 142–152.

Tho, K.K., Chen, Z., Leung, C.F., Chow, Y.K., 2013. Pullout behavior of plate anchor in clay with linearly increasing strength. Can. Geotech. J. 51, 92–102.

Vanmarcke, E.H., 1977. Probabilistic modeling of soil profiles. J. Geotech. Eng. Div. 103 (11), 1227–1246.
Wang, D., Hu, Y., Randolph, M.F., 2010. Three-Dimensional large deformation finite-element analysis of plate anchors in uniform clay. J. Geotech. Geoenviron. 136 (2), 355–365.
Wilde, B., Treu, H., Fulton, T., 2001. Field testing of suction embedded plate anchors. In: The Eleventh International Offshore and Polar Engineering Conference. OnePetro.
Xing, G., Zhang, L., Xuan, W., Ma, J., Ye, X., Guo, S., Liu, Y., 2021. Capacity of double-plate vertically loaded anchor in saturated marine fine sand. Mar. Georesour. Geotechnol. 1–14.
Yang, M., Murff, J.D., Aubeny, C.P., 2010. Undrained capacity of plate anchors under general loading. J. Geotech. Geoenviron. 136 (10), 1383–1393.
Yi, J.T., Huang, L.Y., Li, D.Q., Liu, Y., 2020. A large-deformation random finite-element study: failure mechanism and bearing capacity of spudcan in a spatially varying clayey seabed. Géotechnique 70 (5), 392–405.
Yu, L., Liu, J., Kong, X., Hu, Y., 2011. Numerical study on plate anchor stability in clay. Géotechnique 61 (3), 235–246.
Yu, S.B., Hambleton, J.P., Sloan, S.W., 2015. Undrained uplift capacity of deeply embedded strip anchors in non-uniform soil. Comput. Geotech. 70, 41–49.
Zhang, N., Matthew Evans, T., Zhao, S., Du, Y., Zhang, L., 2020. Discrete element method simulations of offshore plate anchor keying behavior in granular soils. Mar. Georesour. Geotechnol. 38 (6), 716–729.
Zhu, H., Griffiths, D.V., Fenton, G.A., Zhang, L.M., 2015. Undrained failure mechanisms of slopes in random soil. Eng. Geol. 191, 31–35.